Metal-insulator transition in a disordered and correlated $SrTi_{1-x}Ru_xO_3$ system: Changes in transport properties, optical spectra, and electronic structure

K. W. Kim, J. S. Lee, and T. W. Noh*
School of Physics and Research Center for Oxide Electronics, Seoul National University, Seoul 151-747, Korea

S. R. Lee and K. Char
School of Physics and Center for Strongly Correlated Materials Research, Seoul National University, Seoul 151-747, Korea
(Received 22 September 2004; published 7 March 2005)

We investigated the transport and optical properties of $SrTi_{1-x}Ru_xO_3$ ($0 \leqslant x \leqslant 1$) which shows a metal-insulator transition at x about 0.5 at room temperature. While $SrRuO_3$ is a ferromagnetic metal with 4 t_{2g} electrons, $SrTiO_3$ is a band gap insulator with an optical gap of about 3.7 eV. Because the t_{2g} states of Ru and Ti are well decoupled, the electronic structure of $SrTi_{1-x}Ru_xO_3$ near the Fermi level is dominated by Ru t_{2g} states. The temperature dependent transport data of samples near the transition showed characteristics of various localization phenomena. The optical conductivity spectra showed that as $SrTi_{1-x}Ru_xO_3$ changes from a metal to an insulator, the Drude-like peak decreases and evolves into an incoherent peak, which shifts to higher energy gradually and disappears. This evolution of the optical conductivity could not be explained by either disorder or correlation mechanisms. From our transport and optical data, we could categorize six kinds of electronic states in this system depending on x: a correlated metal ($x \sim 1.0$), a disordered metal ($x \sim 0.7$), an Anderson insulator ($x \sim 0.5$), a soft Coulomb gap insulator ($x \sim 0.4$), a disordered correlation insulator ($x \sim 0.2$), and a band insulator ($x \sim 0.0$). To understand these electronic structure evolutions, the disorder and the electron correlation effects should be considered together. We believe that $SrTi_{1-x}Ru_xO_3$ is a prototype system experiencing a Mott-Hubbard like transition in the Ru t_{2g} alloy band, which is derived from the combined effects of the disorder and the electron correlation.

DOI: 10.1103/PhysRevB.71.125104 PACS number(s): 78.20.−e, 73.61.−r, 78.40.−q, 78.66.−w

I. INTRODUCTION

Metal-insulator transition (MIT) is a fundamental and practically useful phenomenon in condensed matter science. Numerous mechanisms, including carrier doping, electron-phonon coupling, electron correlation, and disorder, have been proposed. Among them, two MIT mechanisms have attracted lots of attention from the condensed matter community due to their intriguing nature. One is called an Anderson transition, which can result from the localization of the one-electron wave function under a strong random potential.[1,2] The effect of the random potential has usually been treated as a disorder effect. The other is called a Mott-Hubbard transition, which can be attributed to strong Coulomb interaction between electrons, resulting in an insulating state even in a system with a partially filled band.[3] The electron-electron interaction has usually been treated as a correlation effect. During the last several decades, there have been lots of theoretical and experimental efforts to investigate the detailed features of those transitions.

It should be noted that, in numerous materials, both the disorder and the correlation effects can appear at the same time. The strong correlation effect between electrons has provided us lots of intriguing phenomena near MIT, such as high transition temperature superconductivity,[4] colossal magnetoresistance,[5] numerous spin/charge/orbital orderings,[6] and so on. These phenomena have usually been treated by considering the correlation effect only, for example, by using the Mott-Hubbard Hamiltonian. However, real materials are always subject to numerous kinds of disorder, such as impurities, vacancies, nonhomogeneous chemical distribution, and/or nonstoichiometric composition. Therefore, it is very important to understand the combined effects of disorder and electron interaction.

Recently, there have been lots of theoretical efforts[7–13] to investigate systems with disorder and electron correlation using the Anderson-Hubbard Hamiltonian

$$H = -t \sum_{\langle i,j \rangle \sigma} c_{i\sigma}^{\dagger} c_{j\sigma} + U \sum_{i} n_{i\uparrow} n_{i\downarrow} + \sum_{i\sigma} \epsilon_i n_{i\sigma}, \qquad (1)$$

where $c_{i\sigma}^{\dagger}$ ($c_{i\sigma}$) is the creation (annihilation) operator for a spin-σ electron at site i, t is the hopping integral for the electrons between nearest-neighbor sites, U is the on-site Coulomb repulsion energy, $n_{i\sigma} = c_{i\sigma}^{\dagger} c_{i\sigma}$ is the local electron number operator, and ϵ_i is a random site potential which has some independent distribution with variance Δ^2 and gives disorder of strength Δ in the system. The first hopping integral term represents the kinetic energy contribution, resulting in the bandwidth W. The second term represents the correlation energy contribution. Note that these two terms form the Mott-Hubbard Hamiltonian. The third term takes account of the disorder contribution.

Using the Hamiltonian, given in Eq. (1), numerous intriguing phenomena have been theoretically predicted near the MIT. For example, if electrons in a disordered insulator begin to interact with each other, the disorder strength can be renormalized,[7] resulting in some physical characteristics different from those of the free ($U=0$) disordered case.[9,10] On the other hand, when disorder is introduced in a Mott insu-

lator, then the Δ term makes the Hubbard bands broaden to narrow the correlation gap and could even lead to closure of it to make the system into a Mott glass.[11] In addition, the combination of the Δ and U terms could induce strong scattering, which strongly suppresses development of the quasicoherent energy scale, already in the metallic state.[12]

In contrast to these fascinating progresses in theories, there have been few experimental efforts to systematically investigate the combined effects of disorder and electron correlation. One of the reasons is that it would be difficult to find a system with the required conditions of $\Delta \sim U$ and a reasonable simplicity in its electronic structure. For most strongly disordered semiconductors,[14,15] the disorder and the kinetic terms could be large but $U \ll (\Delta, W)$. For most perovskite transition metal oxides with an *A*-site disorder, the *A*-site metal ions do not contribute to form the conducting network, so the Δ term usually is not large enough to satisfy the required condition, and $\Delta \ll (U, W)$. For example, numerous experimental works on $(Ca,Sr)VO_3$ and $(Ca,Sr)_2RuO_4$ did not take account of the cation disorder at the *A* site in explaining their physical properties.[16,17] On the other hand, for some transition metal oxides with a *B*-site disorder, the disorder effect could be large to satisfy the required condition of $\Delta \sim U$, since the *B*-site metal ions are part of the conducting network. For example, the physical properties of $La(Ni,Mn)O_3$ and $La(Ni,Fe)O_3$ were explained in terms of electronic structural changes due to disorder.[18] However, these oxide system are complicated, since both of the constituent *B*-site metal ions have *d* electrons with t_{2g} and e_g characters.

On the other hand, the *B*-site substituted perovskite $SrTi_{1-x}Ru_xO_3$ can be a very interesting system to look into experimentally. $SrTiO_3$, one of the end members, is a simple band gap insulator with a wide band gap of about 3.7 eV.[19,20] Since there is no *d* electron, the oxygen *p* states form the valence bands. The other end member, $SrRuO_3$, is a metal with a ferromagnetic transition at $T_c \sim 160$ K. It has 4 t_{2g} electrons in the low spin configuration. It is widely believed that this ruthenate is a correlated metal located near the boundary of the Mott-Hubbard transition.[21–23] By mixing $SrRuO_3$ with $SrTiO_3$, these two end members can form solid solutions for all the doping region of *x*, and a MIT does occur at $x \sim 0.5$ at room temperature. In the $SrTi_{1-x}Ru_xO_3$ system, both transition metal ions maintain their own valencies of 4+ as in mother materials. And the substitution of Ru^{4+} ions for Ti^{4+} ions puts extra t_{2g} electrons in the d^0 insulator, so its electronic evolution could be simple. In addition, the Ru^{4+} substitution does not accompany any additional phase transition which can affect its electronic structure, which makes $SrTi_{1-x}Ru_xO_3$ an ideal system to systematically investigate the combined effects of disorder and correlation.

Previously, Kostic *et al.* and Dodge *et al.* reported the optical conductivity spectra of $SrRuO_3$, and showed an unconventional frequency dependence of the low energy metallic component.[24,25] And in its paramagnetic state, the conductivity shows a maximum at very low energy comparable with k_BT. To understand these behaviors, various interpretations considering strong electron correlation, local quantum chemical aspects, and disorder have been made.[25–27] However, there is no consensus on the origin of the observed phenomena yet except that electron correlation is important and this material is highly sensitive to disorder. Nevertheless, in a broad context $SrRuO_3$ still could be considered as a representative metallic system with the electron correlation effect. And creating large potential disorder by substituting Ti^{4+} ions for Ru^{4+} ions, we could investigate how the disorder plays its role in this correlated system.

In this paper, we present the transport properties and optical spectra of $SrTi_{1-x}Ru_xO_3$ films $(0 \leq x \leq 1)$. In Sec. II, we will explain the film deposition methods and the experimental techniques for transport and optical measurements. In Sec. III, we will show their temperature-dependent transport properties and how they vary systematically with the Ru doping. We will also show their room temperature optical conductivity and dielectric constant spectra, and point out features in the optical spectra changes. In Sec. IV, we will analyze and discuss our data. We will show that the systematic variations in the physical properties cannot be explained either by the disorder nor by the correlation only, but that both effects should be included. By carefully analyzing the transport and optical properties together, we will divide the doping effects into six different regions and discuss possible electronic structures. We believe that this classification can provide some insights for future studies. In Sec. V, we will summarize our results.

II. EXPERIMENTAL METHODS

$SrTi_{1-x}Ru_xO_3$ films were grown by pulsed laser ablation on $SrTiO_3(100)$ substrates. A multilayer deposition technique was used to realize the intermediate compounds by depositing alternative amounts of materials corresponding to less than one unit cell from two end member targets.[28] The films were deposited at 700 °C under 100 mTorr oxygen pressure. The growth rates for $SrRuO_3$ and $SrTiO_3$ were 0.05 and 0.1 Å/pulse, respectively. The quantity of Ru^{4+} ions *x* was determined by the ratio of the number of pulses on each target weighted by the growth rate. Films were grown to be 10–30 nm thick, in which thickness range the variations of their transmission spectra were found to be large enough to see the variations in the optical measurements.

For each *x* value, two kinds of films were deposited simultaneously. The large-sized films were used for optical measurements and the other ones were used for dc transport and thickness measurements. The conventional four-probe method was used for dc transport measurements. Complex optical constants $\tilde{\sigma}$ of the $SrTi_{1-x}Ru_xO_3$ thin films were determined in a wide frequency range from 0.2 to 5.0 eV by combining two methods. In the low frequency transparent region from 0.2 to 3.1 eV, $\tilde{\sigma}(\omega)$ were obtained from reflectance and transmittance spectra using the numerical inversion technique, called the intensity transfer matrix method (ITMM).[29] And, for the higher frequency above 1.5 eV, $\tilde{\sigma}(\omega)$ was determined with spectroscopic ellipsometry. At low frequencies below 0.2 eV, the opaque substrate due to phonon responses did not allow us to measure optical spectra in that region. In these methods, the Kramers-Kronig analysis and associated extrapolation procedures were not required. We

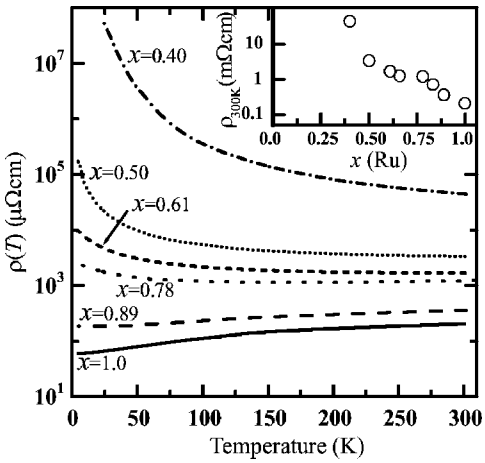

FIG. 1. Temperature dependent dc transport data $\rho(T)$ and $\rho(300\ \mathrm{K})$ in the inset. $\rho(T)$ shows composition-dependent MIT as x decreases. For $x<0.4$, the resistance was too high to be measured.

found that $\tilde{\sigma}(\omega)$ from both methods matched quite well in the overlapping frequency region.

III. RESULTS

A. dc transport properties

Figure 1 shows temperature (T)-dependent dc resistivity curves $\rho(T)$ of the $SrTi_{1-x}Ru_xO_3$ films. For $x>0.8$, $d\rho/dT>0$ at all measured temperatures, which corresponds to a metallic behavior. As x decreases, $\rho(T)$ increases and enters intriguing insulating states. For $x\sim0.7$, $\rho(T)$ shows a T-dependent change from a metallic behavior ($d\rho/dT>0$) in the high-T region to an insulatorlike behavior ($d\rho/dT<0$) in the low-T region.[30,31] For $x\leqslant0.5$, $d\rho/dT<0$ at all temperature, which indicates that it is in an insulating state. For $x<0.4$, $\rho(T)$ could not be measured due to very high values of the resistance. The inset of Fig. 1 shows a plot of $\rho(300\ \mathrm{K})$ vs x. A large change in $\rho(300\ \mathrm{K})$ occurs at $x\sim0.5$. At room temperature, the doping dependent metal-insulator transition seems to occur at $x\sim0.5$, which was estimated from $d\rho/dT$ and $\rho(300\ \mathrm{K})$. It should be noted that another significant change in $\rho(300\ \mathrm{K})$ appears at $x\sim0.8$.

It is well known that the T dependence of $\rho(T)$ provides us lots of insights on the nature of MIT, especially related to the disorder. In the three-dimensional (3D) weak localization regime,[2,32] at low temperature, $\rho(T)$ should behave as

$$\frac{1}{\rho(T)}=\frac{1}{\rho_0}+\frac{e^2}{\hbar\pi^3 a}T^{1/2}. \tag{2}$$

As we already mentioned earlier, $\rho(T)$ of $x\sim0.7$ shows a T-dependent change from a metallic to an insulatorlike behavior. The low-T behaviors, shown in Fig. 2(a), provide reasonably good agreement with Eq. (2).

When the disorder effect becomes larger, the Mott-type variable range hopping (VRH) conduction mechanism has been known to play an important role. Figure 2(b) shows $\rho(T)$ of $x=0.5$, which obeys the following Mott VRH equation:[2,33–35]

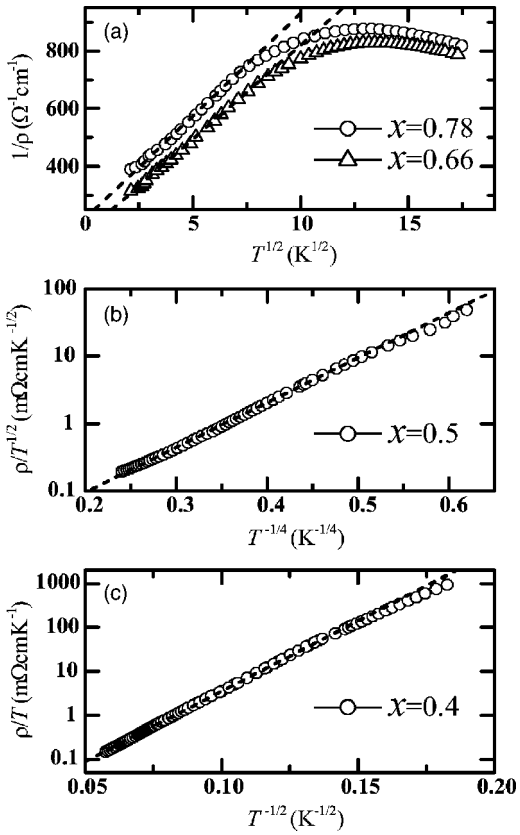

FIG. 2. dc transport data with various localization strength. (a) Samples of $x\sim0.7$ show 3D weak localization transport phenomena with a change in the sign of $d\rho(T)/dT$ at low temperature. And (b) at $x=0.5$ the Mott-type VRH, (c) at $x=0.4$ the E-S VRH conduction behaviors are observed (see Ref. 35).

$$\rho(T)=A\sqrt{T}\exp\left[\left(\frac{T_M}{T}\right)^{1/4}\right]. \tag{3}$$

In such a state, there should be a finite but localized density of states (DOS) at the Fermi energy E_F. However, mobility edges formed near band edges prevent free motions of carriers. The good agreement between $\rho(T)$ of $x=0.5$ film and Eq. (3) suggests that the sample must be near the boundary of the MIT, which is called a disorder induced Anderson transition.

As the electron correlation effect becomes important in a disordered system, the Efros-Scklovskii VRH (E-S VRH) transport behavior has been frequently observed in numerous systems.[36–38] As shown in Fig. 2(c), for the $x=0.4$ film, $\rho(T)$ can be explained well by the E-S VRH formula

$$\rho(T)=BT\exp\left[\left(\frac{T_{ES}}{T}\right)^{1/2}\right]. \tag{4}$$

This implies that, in the sample of $x=0.4$, the electron correlation, as well as disorder, should be considered as an important ingredient in the evolution of the electronic structure.

B. Optical conductivity spectra

Now let us look into the optical conductivity spectra, $\sigma_1(\omega)$, which were obtained by taking the real part of $\tilde{\sigma}$.

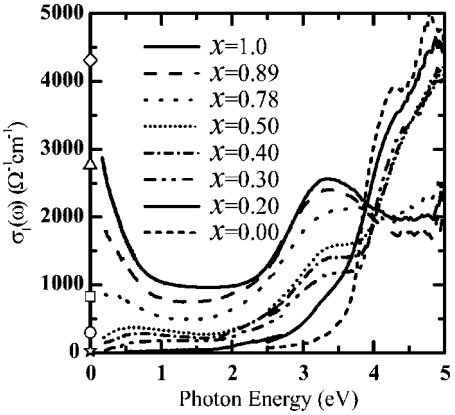

FIG. 3. Optical conductivity spectra $\sigma_1(\omega)$ of $SrTi_{1-x}Ru_xO_3$ are obtained from ITMM calculations and ellipsometry measurements. $\sigma_1(\omega)$ from ITMM are plotted in $0.2\ \text{eV} \leqslant \omega \leqslant 2.7\ \text{eV}$ and from ellipsometry in $2.5\ \text{eV} \leqslant \omega < 5\ \text{eV}$. dc values marked with symbols are of $x=1.0$, 0.89, 0.78, 0.50, and 0.40, respectively, in decreasing order.

Figure 3 shows $\sigma_1(\omega)$ of $SrTi_{1-x}Ru_xO_3$ $(0 \leqslant x \leqslant 1)$ at room temperature in the frequency region of $0.2\ \text{eV} < \omega < 5.0\ \text{eV}$. On the y axis, the dc values, obtained from the transport measurements, were marked as symbols. In $\sigma_1(\omega)$ of the $SrRuO_3$ (i.e., $x=1.0$), two distinct structures, centered at $\omega = 0$ eV and about 3.3 eV, were observed. The former spectral feature should be due to the low energy Drude-like free carrier response, coming from the coherent quasiparticle DOS, existing near E_F. The latter feature has been assigned to the charge-transfer transition from O $2p$ to empty Ru t_{2g} states.[22] On the other hand, in $\sigma_1(\omega)$ of the $SrTiO_3$ film (i.e., $x=0.0$), a strong feature was observed above 4.0 eV. This strong spectral feature has been assigned to the charge transfer transition from O $2p$ states to Ti t_{2g} states.[20]

In $\sigma_1(\omega)$ of the other $SrTi_{1-x}Ru_xO_3$ films, all of the above-mentioned three features could be observed. As x decreases, the spectral weight in the low frequency region below 3.8 eV decreases, suggesting that it must mainly originate from the Ru t_{2g} states. In the meanwhile, the spectral weight in the high frequency region above 3.8 eV increases, implying the importance of the Ti t_{2g} states. These general behaviors can be simply understood in terms of the decrease of Ru^{4+} ions and the increase of Ti^{4+} ions. In addition, the low frequency coherent peak of $SrRuO_3$ continuously decreases and develops into an incoherent peak. These overall spectral weight changes must be related to the doping dependent electronic structural changes, which will be discussed in Sec. IV E.

Figure 4(a) shows a more detailed plot of $\sigma_1(\omega)$ in the low frequency region up to 1.7 eV. To see the spectral behavior changes more clearly, $\sigma_1(\omega)$ was normalized with a value at $\omega=1.7$ eV, i.e., $\sigma_1(1.7\ \text{eV})$. As x decreases, the Drude-like peak decreases and a conductivity maximum appears at a finite frequency, which moves to a higher frequency. This conductivity shape is similar with the characteristic $\sigma_1(\omega)$ behavior of a highly disordered system.[39–42] Figure 4(b) shows the corresponding dielectric constant spectra $\epsilon_1(\omega)$. Just like the dc transport properties, both $\sigma_1(\omega)$ and $\epsilon_1(\omega)$ show systematic changes with the transition metal ion substitution.

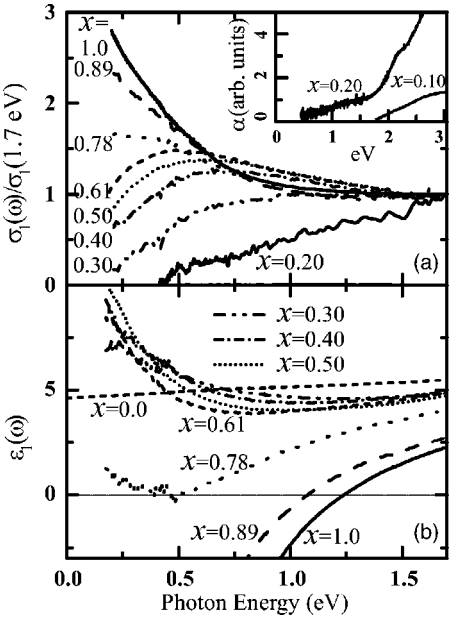

FIG. 4. Low frequency behaviors of $SrTi_{1-x}Ru_xO_3$. (a) Normalized conductivity $\sigma_1(\omega)$ to $\sigma_1(1.7\ \text{eV})$ show that a peaklike structure develops as x decreases and (b) dielectric constant $\epsilon_1(\omega)$ show a deep structure which is closely related with the peaklike structure in $\sigma_1(\omega)$. For $x=0.0$ the phonon contribution to $\epsilon_1(\omega)$ is subtracted. The inset shows absorption spectra of $x=0.20$ and 0.10. For $SrTi_{0.9}Ru_{0.1}O_3$, no d-d transition feature is observed.

Both $\sigma_1(\omega)$ and $\epsilon_1(\omega)$ for $x>0.8$ show typical metallic responses: as ω decreases, $\sigma_1(\omega)$ increases in the low frequency region, and $\epsilon_1(\omega)$ decreases and becomes negative. For $x \sim 0.7$, $\sigma_1(\omega)$ at low frequency decreases to become a broad structure, and $\epsilon_1(\omega)$ at low frequency increases and is not negative any more. Although the general shape of $\sigma_1(\omega)$ is still broadly centered around zero frequency, the nonnegative value of $\epsilon_1(\omega)$ suggests that its electrodynamic response should be different from that of free carriers. For $x=0.5$, $\sigma_1(\omega)$ seems to have a broad peak in the midinfrared region and $\epsilon_1(\omega)$ seems to become large in the low frequency region. An increase of low frequency ϵ_1 has been observed in numerous systems near the MIT.[43–45] As we have already concluded from the dc transport behavior, this confirms that the MIT of this system occurs at x about 0.5. For $x=0.4$ and 0.3, the general behaviors of $\sigma_1(\omega)$ and $\epsilon_1(\omega)$ are quite similar to those for $x=0.5$. However, it looks like that simple linear extrapolations of $\sigma_1(\omega)$ of the samples for $x=0.5$, 0.4, and 0.3 to the zero frequency limit provide different crossing points with the y axis. [For $x=0.5$, this would provide a positive value of $\sigma_1(0\ \text{eV})$. For $x=0.3$, $\sigma_1(\omega)$ would become zero at a positive frequency, so this sample seems to have an energy gap.] For $x=0.2$, $\sigma_1(\omega)$ clearly demonstrates an optical gap of about 0.4 eV, which is also evident in the absorption spectra, shown in the inset of Fig. 4(a). For $x=0.0$, there is no absorption and $\epsilon_1(\omega)$ becomes nearly constant below 1.7 eV.

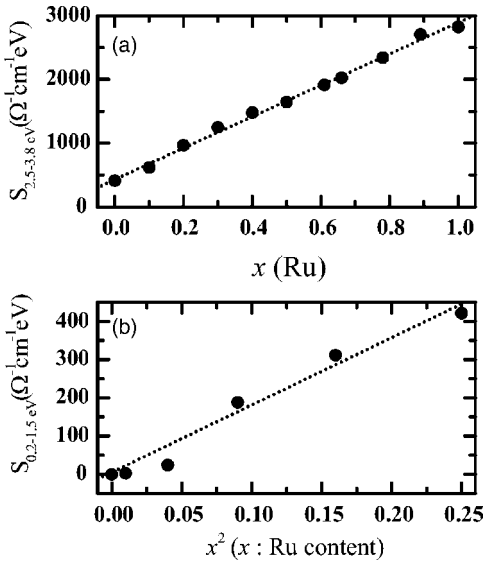

FIG. 5. (a) Spectral weight of the *p-d* transition from O 2*p* states to empty Ru t_{2g} states centered at $\omega \sim 3.3$ eV and (b) of the intersite *d-d* transition of insulating samples.

IV. ANALYSIS AND DISCUSSION

A. Spectral weight analyses

To obtain some more insights on the nature of the low-frequency spectral features of the $SrTi_{1-x}Ru_xO_3$ films, we performed spectral weight analyses. Figure 5(a) shows the spectral weight near the 3.3 eV feature by integrating $\sigma_1(\omega)$ from 2.5 to 3.8 eV. Note that the spectral weight seems to be linearly proportional to x. Optical conductivity $\sigma_1^{ij}(\omega)$ over an interband transition region and its spectral weight are proportional to the joint density of states $J^{ij}(\omega)=\int d\varepsilon n_v^i(\varepsilon)n_c^j(\varepsilon+\hbar\omega)$.[46] Since the DOS of the O 2*p* states, $n_v(\omega)$, does not change much with x, the linear dependence of spectral weight on x, shown in Fig. 5(a), might come from the increase of the Ru^{4+} ions, i.e., from the increase of the Ru t_{2g} DOS in $n_c(\omega)$. This indicates that the spectral feature around 3.3 eV should be attributed solely to the transition from the O 2*p* to the empty Ru t_{2g} states in this doped system. This result agrees with earlier reports that the t_{2g} bands of Ru and Ti are well separated.[47,48] From these facts, we can also expect that the Ti t_{2g} contribution should show up mainly at the energy region higher than 3.3 eV. Figure 5(b) shows the low frequency spectral weights, which were obtained by integrating $\sigma_1(\omega)$ from 0.2 to 1.5 eV. Note that this spectral weight seems to be proportional to x^2, whose x dependence suggests that this spectral feature might come from the intersite transition between Ru t_{2g} states.

B. Effects of disorder

1. Macroscopic inhomogeneities: The effective medium approximation

Some previous studies presented an abrupt resistivity change at $x \sim 1/3$ and Abbate *et al.* suggested that the MIT of $SrTi_{1-x}Ru_xO_3$ should be a percolation transition like that of metals embedded in a rare gas matrix.[48,49] If such macroscopic scale inhomogeneities determine the MIT, our optical conductivity spectra can be described by the effective medium approximation (EMA).[45] Note that the EMA is an effective medium theory, which can explain the average response of the inhomogeneous medium in terms of the volume fractions and macroscopic dielectric properties of the constituents.

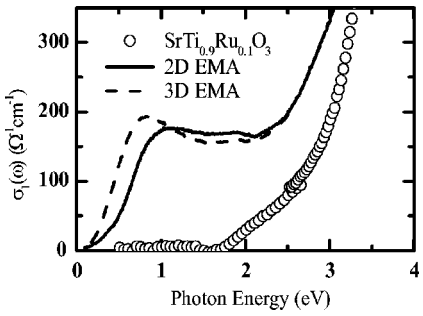

FIG. 6. Comparison with 2D and 3D EMA calculations for $SrTi_{0.9}Ru_{0.1}O_3$.

It was found that the EMA cannot explain our optical spectra. As an example, in Fig. 6, we plotted the predictions of two- and three-dimensional (2D and 3D) EMAs for $\sigma_1(\omega)$ for the $SrTi_{0.9}Ru_{0.1}O_3$ sample. The 2D and the 3D EMAs assume that that constituent materials have 2D cylindrical and 3D spherical shapes, respectively.[45] As shown in Fig. 6, the EMAs predict very broad impurity bands at all the frequencies below the optical gap of $SrTiO_3$, i.e., about 3.7 eV. However, the experimental spectra showed the behavior of an optical gap, located at 1.7 eV. Such qualitative disagreements between our experimental data and the EMAs' predictions can be found for all values of x, except for the end members. This observation is in agreement with our earlier magnetization studies, which showed that our films should be homogeneous on the macroscopic scale.[28] In addition, the studies showed that their magnetic properties could be explained by assuming a random distribution of the substituted sites.[28]

2. Microscopic disorder: The localization modified Drude model

As we have already mentioned, the overall spectral behaviors of our $SrTi_{1-x}Ru_xO_3$ films have some similarities with those of a microscopically disordered system. One phenomenological model to explain the effect of disorder on $\sigma_1(\omega)$ is the localization modified Drude (LMD) model,[41] expressed by

$$\sigma_1(\omega) \approx \sigma_D(\omega)\left\{1-\frac{1}{(k_F l)^2}[1-(3\tau\omega)^{1/2}]\right\}. \qquad (5)$$

Here $\sigma_D(\omega)[=\omega_p^2\tau/4\pi(1+\omega^2\tau^2)]$, k_F, and l are the Drude conductivity, the Fermi wave vector, and the mean free path for carriers inside a metal, respectively. And ω_p and $1/\tau$ in $\sigma_D(\omega)$ are the plasma frequency and the scattering rate of carriers. In this model, $k_F l$ and $1/\tau$ are important fitting parameters related to the localization behavior. $\sigma_1(\omega)$ of some polymer systems with a peak structure in the mid-infrared

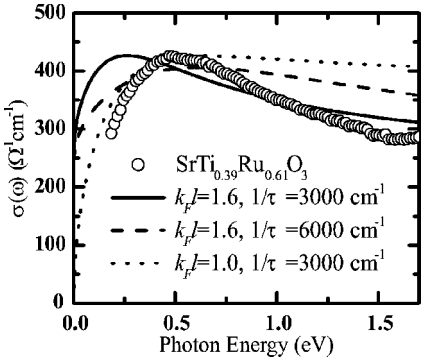

FIG. 7. Comparison with the LMD model. Figure shows model fittings with a few parameter sets to $\sigma_1(\omega)$ of the $x=0.61$ sample, all of which do not agree with the data.

region has been well explained by the LMD model.[41] In the LMD model, the frequency of the conductivity maximum ω_{peak} is dependent on both $1/\tau$ and $k_F l$. Also, the increase of ω_{peak} results from the increase of $1/\tau$ and/or the decrease of $k_F l$, which implies that the disorder effect becomes stronger. The low frequency spectra of the $SrTi_{1-x}Ru_xO_3$ system show that such a peak develops from the Drude-like peak of $SrRuO_3$ and continues to increase. And this behavior can be understood qualitatively as being due to the increasing disorder effect.

However, there are some limitations in applying the LMD model to the $SrTi_{1-x}Ru_xO_3$ system. In the beginning, we tried to fit our optical spectra using the Drude model for $\sigma_D(\omega)$, but failed with physically reasonable parameter values of k_F and l. Then we noticed that $\sigma_1(\omega)$ for the metallic mother material $SrRuO_3$ cannot be described by the Drude model.[24,25] Previously Dodge *et al.* pointed out such a non-Fermi-liquid behavior for $SrRuO_3$ and proposed a fractional power law behavior such that $\sigma_1(\omega)=A/(\tau^{-1}-i\omega)^{0.5}$.[24] So, we tried the fractional power law behavior for $\sigma_D(\omega)$ and applied the LMD model. Figure 7 shows some model fitting results for the $x=0.61$ sample. With $k_F l=1.6$ and $1/\tau=3000\ \mathrm{cm}^{-1}$, the fitting curve shows a comparable peak width around the conductivity maximum but the peak is located at a lower frequency. By increasing $1/\tau$ the peak position moves to a higher frequency but the peak feature becomes too broad. For a smaller $k_F l$ value, a better fitting curve could be obtained in the spectral region for $\omega \lesssim \omega_{peak}$, but it deviated too much for $\omega > \omega_{peak}$. This failure of the LMD model and the evolution to an insulating phase with a finite gap feature, displayed in Fig. 4(a), imply that other mechanisms should be included to explain the physics of $SrTi_{1-x}Ru_xO_3$.

C. Effects of correlation: The extended Drude model analysis

$SrRuO_3$ is known as a correlated metallic compound near the boundary of a Mott-Hubbard transition, where electron correlation is reasonably high.[21–23] To investigate how the correlation affects the electrodynamics of $SrTi_{1-x}Ru_xO_3$, we used the extended Drude model.[25,50] In this model, the scattering rate and effective mass in the free carrier Drude response could be modified due to the electron correlation effect as follows:

$$\tilde{\sigma}(\omega) = \frac{\omega_p^2}{4\pi}\frac{\tau(\omega)}{[1 - i\omega m^*(\omega)\tau(\omega)]}, \tag{6}$$

where $1/\tau(\omega)$ and $m^*(\omega)$ represent the frequency dependent scattering rate and effective mass enhancement, respectively. Using the experimental $\tilde{\sigma}(\omega)$, we applied the extended Drude model to the $SrTi_{1-x}Ru_xO_3$ samples in the metallic region.

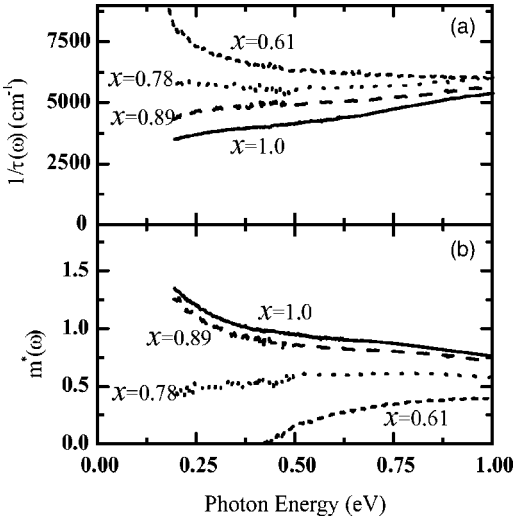

FIG. 8. (a) Scattering rate and (b) mass enhancement from extended Drude analysis for metallic states of $x=1.0$, 0.89, 0.78, and 0.61.

Figures 8(a) and 8(b) show $1/\tau(\omega)$ and $m^*(\omega)$ from the extended Drude model analysis, respectively. For $x=1.0$ and 0.89, as ω decreases, $1/\tau(\omega)$ decreases and $m^*(\omega)$ increases, which are characteristic behaviors of a strongly correlated metal.[25,50] This strongly points out that the correlation effect should be important in the electrodynamics of $SrTi_{1-x}Ru_xO_3$. However, for $x=0.61$, whose $\rho(T)$ response is metallic at room T but insulatorlike at low T, the analysis based on the extended Drude model fails. As shown in Fig. 8(b), $m^*(\omega)$ becomes negative, which is just the opposite to our intuition. This indicates that the extended Drude model should be applied carefully for a system where both the disorder and the correlation effects play together.

D. Coexistence of disorder and correlation effects

To understand the physical properties of $SrTi_{1-x}Ru_xO_3$, we should take account of the coexistence of the disorder and the correlation effects. The disorder effect manifests itself in various transport behaviors of the $x=0.4-0.7$ samples, as shown in Fig. 2. Note that the E-S VRH behavior for the $x=0.4$ sample also suggests that the correlation should also play an important role for this sample. On the other hand, the correlation effect could be confirmed from the mass enhancement behaviors in the optical spectra of the $0.8<x\leqslant 1$ samples, as shown in Fig. 8. In addition, as shown in Sec.

TABLE I. Summary of the states and their characteristics observed in $SrTi_{1-x}Ru_xO_3$.

	Insulator				Metal	
	Band insulator	Disordered correlation insulator	Soft Coulomb gap insulator	Anderson insulator	Disordered metal	Correlated metal
x	$x\sim 0$	$x\sim 0.2$	$x\sim 0.4$	$x\sim 0.5$	$x\sim 0.7$	$x\sim 1.0$
$\sigma(\omega)$	Wide optical gap	Reduced gap	(Soft Coulomb gap)	Peaklike low energy structure	Broad incoherent response	Drude-like coherent peak
$\rho(T)$	Thermal excitation	Thermal excitation	Hopping conduction (E-S VRH)	Hopping conduction (Mott VRH)	3D weak localization	Metallic
	$\rho_0 \exp(T_G/T)$	$\rho_0 \exp(T_G/T)$	$BT\exp[(T_{ES}/T)^{1/2}]$	$A\sqrt{T}\exp[(T_M/T)^{1/4}]$	$[1/\rho_0+(e^2/\hbar\pi^3 a)\sqrt{T}]^{-1}$	$d\rho/dT>0$

IV B 2, the optical spectra of the $x=0.61$ sample resemble the optical spectra of disordered samples, suggesting that the disorder could play an important role.

In the $SrTi_{1-x}Ru_xO_3$ system, the low energy physics near E_F could be dominated by the Ru t_{2g} states. The simple substitution of Ru^{4+} ions for Ti^{4+} ions puts extra t_{2g} electrons in the d^0 insulator of $SrTiO_3$, so its random substitution can be treated as altering the potential to have the following distribution:

$$\mathcal{P}(\epsilon_i) = x\,\delta(\epsilon_i - \epsilon_{Ru}) + (1-x)\,\delta(\epsilon_i - \epsilon_{Ti}). \tag{7}$$

Then, the above distribution should produce disorder of strength $\Delta_0 = \epsilon_{Ti} - \epsilon_{Ru}$ in the system.[51] If we use the values of the end members,[19–22] Δ_0 can be estimated to be about 1.7–2.1 eV, which is comparable to the U value (i.e., about 1.5–2.0 eV[21,22,52]) of $SrRuO_3$. For $SrRuO_3$, it is free from the disorder and its correlation energy U should be just a little smaller than the critical value U_c, since the ruthenate is well known to be located close to MIT.[21–23] How should the correlation term be affected by the Ti doping in the other $SrTi_{1-x}Ru_xO_3$ system?

As x decreases, the Ru t_{2g} band width W will decrease due to the increase of the average Ru-Ru distance.[9,53,54] In addition, according to the coherent potential approximation (CPA), which is the most frequently used theoretical method in investigating the Anderson-Hubbard Hamiltonian for a bi-alloy system of $A_{1-x}B_x$ with alloy bands separated,[12,53–55] the bandwidth of the substituent element B should be renormalized by a factor $\sqrt{x}$.[9,53,54] On the other hand, U does not change much with x, since the electron correlation is a local property. Therefore, as x decreases, the renormalized correlation strength U/W in $SrTi_{1-x}Ru_xO_3$ is expected to increase. This fact, together with $U\sim\Delta_0$, strongly suggests that both the disorder and the correlation effects should play important roles in the physical properties of $SrTi_{1-x}Ru_xO_3$.

E. Detailed analysis based on $\rho(T)$ and $\tilde{\sigma}(\omega)$

The Ti substitution of the $SrTi_{1-x}Ru_xO_3$ system can be conjectured to be a process of taking out correlated electrons in a random fashion, so the disorder and the correlation effects should play together. Unfortunately, detailed theoretical works on the physical properties of a system with both disorder and correlation are still lacking: for example, we do not have yet a counterpart of the extended Drude model or the localization modified Drude model. Therefore, the systematic changes observed in our transport and optical data on the $SrTi_{1-x}Ru_xO_3$ films can provide some insights for future studies.

In this section, we will divide the system into 6 substitution regions in terms of decreasing x, and look into the detailed behaviors of $\rho(T)$ and $\tilde{\sigma}(\omega)$ in each region. Based on these data, we will discuss the possible electronic structure in each region. A summary of the $\rho(T)$ and $\tilde{\sigma}(\omega)$ behaviors in each region will be given in Table I. And, the electronic structures of the $SrTi_{1-x}Ru_xO_3$ will be summarized in the schematic diagrams of Fig. 9.[56]

1. Correlated metallic region ($0.8<x\leqslant 1$)

Our $SrTi_{1-x}Ru_xO_3$ thin films in this x region seem to show the responses of a metallic system with correlated electrons. Figure 1 shows that $\rho(T)$ is metallic with $d\rho/dT>0$. Capogna *et al.* showed that $\rho(T)$ of $SrRuO_3$ has T^2 dependence below 10 K,[27] a typical response of a correlated electron system. Figures 3 and 4 also showed that, for the $x=1.0$ and 0.89 samples, $\sigma_1(\omega)$ have the Drude-like response in the low frequency region and $\epsilon_1(\omega)$ become negative as $\omega\to 0$, which is a typical response of quasiparticles. The extended Drude model analysis, as displayed in Fig. 8, shows mass enhancement, indicating an active role of correlation for the quasiparticles.

The electronic structure of the samples in the correlated metallic region is schematically shown in Fig. 9(a). The fully occupied O $2p$ band should be located at the lower energy than the Ru t_{2g} band. The t_{2g} band should be partially filled, and there should a quasiparticle peak at E_F. The existence of the peak is due to the electron correlation effect, and similar quasiparticle peaks have been observed in other correlated metals, such as $CaRuO_3$, and $Ca_{1-x}Sr_xVO_3$.[3,17] The schematic diagram also agrees with photoemission and x-ray absorption studies on $SrRuO_3$.[22]

2. Disordered metallic region ($x\sim 0.7$)

The $SrTi_{0.22}Ru_{0.78}O_3$ thin film shows quite intriguing features. As shown in Fig. 1, $\rho(T)$ remains metallic at room T

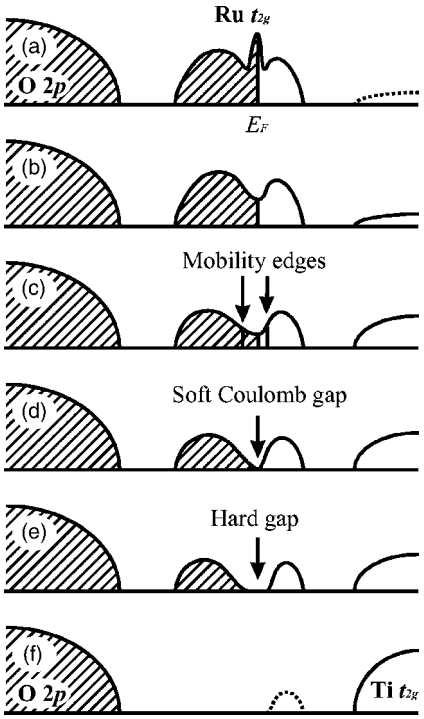

FIG. 9. A schematic diagram for $SrTi_{1-x}Ru_xO_3$. As x decreases, (a) DOS of a correlated metal ($x\sim1$) shows (b) suppression in the correlated quasiparticle peak first due to disorder (a disordered metal, $x\sim0.7$). With further decrease of x, (c) mobility edges are formed near E_F (an Anderson insulator, $x\sim0.5$) and (d) the increased Coulomb interaction results in a soft Coulomb gap at E_F (a soft Coulomb gap insulator, $x\sim0.4$). (e) Finally the disorder induced correlation opens a hard gap (a disordered correlation insulator, $x\sim0.2$). And further decrease of x makes the system (f) a band insulator with a wide optical gap ($x\sim0$).

but insulatorlike ($d\rho/dT<0$) at low T. As shown in Fig. 2(a), its low temperature behavior follows the predicted T dependence for the 3D weak localized regime, shown in Eq. (2). As shown in Fig. 4(a), the $\sigma_1(\omega)$ of the $x=0.78$ sample shows a very broad Drude-like peak. [We also measured $\sigma_1(\omega)$ for the $x=0.66$ sample and found that the results were similar to those for the $x=0.78$ sample.] However, it does not represent the quasiparticle peak: $\epsilon_1(\omega)$ does not go to negative anymore at low frequency. Laad *et al.*[12] calculated $\sigma_1(\omega)$ of a system with moderate disorder and obtained results similar to those of our sample with $x\sim0.7$. Following this calculation, it looks like the scattering becomes strong enough to destroy the low energy coherence and to result in the broad incoherent response of $\sigma_1(\omega)$. The abrupt increase of ρ(300 K) at $x\sim0.8$, observed in the inset of Fig. 1, might have some relation with the disappearance of the coherent quasiparticle peak. The nature of this doping region is not fully understood yet.

The electronic structure in the disordered metallic region is schematically shown in Fig. 9(b). Just like Fig. 9(a), there will be the Ru t_{2g} band near E_F. (Strictly speaking, this band should have characteristics of the Ru t_{2g} and the O $2p$ bands due to the hybridization of these two bands. However, the Ru t_{2g} character should be stronger for the band near E_F.) Note that, in this substitution region, the correlation peak at E_F should be absent. Also, the Ti substitution will provide some states much above the Ru t_{2g} band.

3. Anderson insulator region ($x\sim0.5$)

As shown in Fig. 2(b), $\rho(T)$ of the $x=0.5$ sample shows the Mott VRH behavior, suggesting that it is in an insulating state, called the Anderson insulator. In this state $\sigma_1(\omega)$ is expected to have a specific ω dependence at very low energy as $\sigma_1(\omega)\propto\omega^{1/3}$.[57,58] Although we could not measure optical spectra below 0.2 eV due to the strong multiphonon absorption process in the $SrTiO_3$ substrate, the low frequency behavior of $\sigma_1(\omega)$ is different from that for the $x>0.65$ samples: Fig. 4(a) shows a downturn of $\sigma_1(\omega)$ as ω decreases. In addition, from a simple extrapolation of $\sigma_1(\omega)$ to a zero frequency, we can guess that the optical gap might not exist for this sample. As we already mentioned, the low frequency value of $\epsilon_1(\omega=0.2\text{ eV})$ in Fig. 4(b) shows a maximum near $x=0.5$, which indicates that $SrTi_{0.5}Ru_{0.5}O_3$ is at the boundary of the MIT in this system.[43,44]

The electronic structure of the Anderson insulator is schematically shown in Fig. 9(c). The Mott VRH behavior suggests that mobility edges should be formed near E_F.[1,2] Although there is no energy gap, the electronic states within the mobility edges should be localized, resulting in the insulating behavior. The broad peak structure in $\sigma_1(\omega)$ could be understood in terms of an optical transition from states below E_F to those above.

4. Soft Coulomb gap region ($0.3\lesssim x\lesssim0.4$)

As shown in Fig. 2(c), $\rho(T)$ of the $x=0.4$ sample can be well explained by the E-S VRH formula. Such a transport phenomenon is expected in a disordered system, where strong Coulomb interaction removes some DOS near E_F, opening a soft Coulomb gap. In this state the single particle DOS becomes parabolic and $\sigma_1(\omega)$ is expected to have a specific ω dependence of $\sigma_1(\omega)\propto\omega/|\ln\omega|$ at very low energy.[2,59] As mentioned earlier, we could not directly observe this far infrared behavior due to the strong multiphonon absorption process in the $SrTiO_3$ substrate. The overall shapes of $\sigma_1(\omega)$ of $x=0.3$ and 0.4 are not much different from that of $x=0.5$, which shows the Mott VRH, at least in the frequency region above 0.5 eV. But significant differences could be observed at the lower frequency. When we made simple extrapolations of $\sigma_1(\omega)$ to the zero frequency region, the way $\sigma_1(\omega)$ fell to zero seemed to be different. Especially, for $x=0.3$, a simple extrapolation could be easily made using the expected frequency dependence for the soft Coulomb gap system. This indicates that the soft Coulomb gap opening due to the combined effects of the disorder and the correlation could occur near E_F. The electronic structure of the insulator with a soft Coulomb gap is schematically shown in Fig. 9(d).

5. Disordered correlation insulator region ($x\sim0.2$)

According to the CPA calculations on a bialloy system of $A_{1-x}B_x$ with alloy bands separated, the bandwidth of the sub-

stituent element B should be renormalized by a factor $\sqrt{x}$.[9,53,54] With the smaller number of electrons coming from the Ru^{4+} ions, it is expected that the bandwidth of the Ru bands near E_F should be smaller, opening an energy gap. As shown in Fig. 4(a) and its inset, $\sigma_1(\omega)$ for the $x=0.2$ sample has an optical gap of about 0.4 eV. In addition, they also show a significant spectral weight in the frequency region much below the $SrTiO_3$ optical gap. We classify this state as a disordered correlation insulator, since the most probable origin for the gap is the electron correlation effect. The electronic structure of the insulator with a hard gap is schematically shown in Fig. 9(e). In this state, there exist some bands originating from the Ru t_{2g} states between the O $2p$ and the Ti t_{2g} bands, and energy gap exists between the Ru bands near E_F. Although we could not measure $\rho(T)$ for the samples in this region, their transport behavior is expected to be of the thermal excitation type.

6. Band insulator region ($0 \leqslant x \lesssim 0.1$)

We think that $SrTi_{0.9}Ru_{0.1}O_3$ is an intriguing system to look into. As shown in the inset of Fig. 4(a), $\sigma_1(\omega)$ for the $x=0.1$ sample has an optical gap of about 1.7 eV. Note that, in Fig. 3, $\sigma_1(\omega)$ of the high x value samples have a strong peak around 3.3 eV, originating from the transition between the O $2p$ and Ru t_{2g} states. The edge of this peak can be estimated to be a little smaller than 2.0 eV, which agrees approximately with the optical gap of $SrTi_{0.9}Ru_{0.1}O_3$. This suggests that $\sigma_1(\omega)$ for the $x \sim 0.1$ sample should also be dominated by the p-d transition between the O $2p$ and Ru t_{2g} states. It is possible that the number of Ru^{4+} ions is small, so the correlation might not be so important in this sample. Therefore, we classify this sample as a band insulator, whose electronic structure is schematically shown in Fig. 9(f). In this figure, the dotted line represents the new state developed by the Ru doping, and the observed optical gap of 1.7 eV should be the transition from the O $2p$ to the newly developed states.

Also $SrTiO_3$, one of the mother materials, is a band insulator with a wide band gap of 3.7 eV. Since there is no d electron, the correlation effect should be negligible. A schematic diagram shown in Fig. 9(f) without the dotted component represents its electronic structure.

F. Comparison with earlier works on $SrTi_{1-x}Ru_xO_3$

Shimizu *et al.* performed the first principle calculation for the electronic structure of the $SrTi_{1-x}Ru_xO_3$ system.[47] They predicted that at small Ru concentration, the deep-level states, which consist of the Ru t_{2g} states, appeared below the middle of the band gap of $SrTiO_3$. In this case the wave functions of the Ru t_{2g} states are localized at the Ru sites. And as x increased to be larger than 0.5, the Ru t_{2g} states became delocalized forming an impurity band, which made the system metallic. These results agree with the CPA predictions for a bialloy system in that the Ru t_{2g} band width decreases as x decreases. However, in this calculation, they did not take account of the correlation effect. Therefore, the features of the transport properties and $\tilde{\sigma}(\omega)$ due to the correlation, as discussed in Sec. IV D, cannot be explained.

Abbate *et al.* performed photoemission spectroscopy and x-ray absorption studies on polycrystalline $SrTi_{1-x}Ru_xO_3$ samples.[48] They claimed that the DOS of the mixed compound $SrTi_{1-x}Ru_xO_3$ should be the same as the linear sum of the DOS of each end member. Namely, they showed that, even in the mixed state, the DOS did not show any sudden changes in the energy position and the bandwidth, but that it only decreased linearly. And they claimed that their studies could support the percolation picture of MIT. However those results are quite different from our optical observations. First, the linearly summed DOS is not compatible with the finite gap structure in $\sigma_1(\omega)$. Note that, compared to the photoemission spectroscopy and x-ray absorption studies, our optical spectroscopy has a much higher energy resolution. We believe that the low resolution of their photoemission and x-ray absorption studies, i.e., about 0.3 and 0.5 eV, respectively, made it difficult to observe the spectral weight changes near E_F, which were clearly observed in $\sigma_1(\omega)$ of Fig. 4(a). Also to test the percolation picture, we applied the EMA simulations in Sec. IV B 1. But this picture based on the macroscopic inhomogeneity could not explain our data. As we showed in this paper, both the disorder and the correlation effects should be included properly to explain the electronic structure changes of $SrTi_{1-x}Ru_xO_3$, schematically displayed in Fig. 9.

G. Comparison with other transition metal oxides with strong disorder and correlation

Recent papers on $CaTi_{1-x}V_xO_3$ and $SrTi_{1-x}V_xO_3$ suggested that their MITs should be simply of the Anderson mechanism due to the development of mobility edges near E_F located in the quasiparticle band. In this scenario, the electron correlation plays its role in causing such a quasiparticle band to be separated from the localized Hubbard subbands. Because they did not observe any evidence for correlation contributions, their conclusions seemed to be quite reasonable. However, our $SrTi_{1-x}Ru_xO_3$ system showed the E-S VRH transport behavior and the evolution of $\tilde{\sigma}(\omega)$ with a gap, which cannot be understood in the scenario only in terms of disorder. Nevertheless, we believe that the electronic structures of those systems should not be different in the overall view. That is, their transport studies could be restricted in a rather narrow doping region where the correlation strength U/W is smaller than the critical value. And with a smaller vanadium concentration, we expect that the correlation effect might reveal its characteristics in those systems too.

Sarma *et al.* reported their photoemission and tunneling data on $La(Ni,Mn)O_3$ and $La(Ni,Fe)O_3$.[18] Although their wide energy scale behaviors, observed by the photoemission, were consistent with the predictions of the dynamic mean field calculation, their tunneling data in the low energy region near E_F did not follow the Mott-Hubbard model. They

observed a cusp structure in the DOS of a disordered metallic state, instead of the resonance peak expected in the Mott-Hubbard model. And the dc conductivity followed $T^{1/2}$ dependence at low temperature. These are consistent with our results for a disordered metallic state of the $x \sim 0.7$ sample, which is lack of the correlated quasiparticle peak at E_F. This work illuminated the low energy features in a highly correlated disordered system and could be complementary to our optical conductivity studies. However, this study was limited to the substitution region around the MIT. And the fact that both transition ions supply both t_{2g} and e_g electrons makes it difficult to understand this system. For example, an insulating $LaNi_{0.8}Mn_{0.2}O_3$ sample showed very complicated features. The tunneling data showed a hard gap of 20 meV at 4.2 K, but it was wiped out already at 10 K. But the photoemission data at 100 K could not be fitted with the DOS shape of the hard gap of linear DOS near E_F even after considering the thermal broadening effect. On the other hand, a cusp shape of $|E-E_F|^{1/2}$ could explain well the photoemission spectra. Also a VRH hopping conduction behavior is observed at high temperature transport. Such complicated behaviors could not be understood in terms of any existing theory.

V. CONCLUSION

We presented the transport and optical conductivity data of $SrTi_{1-x}Ru_xO_3$ thin films over the whole composition range. We showed that our optical conductivity spectra could not be explained either by the disorder only nor by the electron correlation only. The physical properties in the wide composition region could be understood within a combined picture of the disorder and the electron correlation effects. Based on the observed transport and optical conductivity data, we classified $SrTi_{1-x}Ru_xO_3$ into six composition regions and discussed the detailed physical properties and proposed proper electronic structure in each region. This work demonstrates that $SrTi_{1-x}Ru_xO_3$ could be a prototype system, where the combined effects of the disorder and the correlation play important roles.

ACKNOWLEDGMENTS

We would like to thank B. J. Yang and Jaejun Yu for useful discussions. This work was supported by the Ministry of Science and Technology through the Creative Research Initiative program, and by KOSEF through the Center for Strongly Correlated Materials Research. Author K. W. Kim gives special thanks to H. J. Kim.

*Author to whom correspondence should be addressed. Email address: twnoh@phya.snu.ac.kr

[1] P. W. Anderson, Phys. Rev. **109**, 1492 (1958); E. N. Economou and M. H. Cohen, Phys. Rev. Lett. **25**, 1445 (1970).
[2] P. A. Lee and T. V. Ramakrishnan, Rev. Mod. Phys. **57**, 287 (1985).
[3] N. F. Mott, *Metal-Insulator Transitions* (Taylor and Francis, London, 1990); X. Y. Zhang, M. J. Rozenberg and G. Kotliar, Phys. Rev. Lett. **70**, 1666 (1993); A. Georges, G. Kotliar, W. Krauth, and M. J. Rozenberg, Rev. Mod. Phys. **68**, 13 (1996).
[4] J. G. Bednorz and K. A. Müller, Z. Phys. B: Condens. Matter **64**, 189 (1986).
[5] S. Jin, T. H. Tiefel, M. McCormack, R. A. Fastnacht, R. Ramesh, and L. H. Chen, Science **264**, 413 (1994).
[6] Y. Tokura and N. Nagaosa, Science **288**, 462 (2000); M. W. Kim, J. H. Jung, K. H. Kim, H. J. Lee, J. Yu, T. W. Noh, and Y. Moritomo, Phys. Rev. Lett. **89**, 016 403 (2002).
[7] D. Tanasković, V. Dobrosavljević, E. Abrahams, and G. Kotliar, Phys. Rev. Lett. **91**, 066603 (2003); K. I. Wysokiński, Phys. Rev. B **60**, 16 376 (1999).
[8] K. Byczuk, M. Ulmke, and D. Vollhardt, Phys. Rev. Lett. **90**, 196403 (2003).
[9] K. Byczuk, W. Hofstetter, and D. Vollhardt, Phys. Rev. B **69**, 045112 (2004).
[10] V. Janiš and D. Vollhardt, Phys. Rev. B **46**, 15 712 (1992).
[11] E. Orignac, T. Giamarchi, and P. Le Doussal, Phys. Rev. Lett. **83**, 2378 (1999).
[12] M. S. Laad, L. Craco, and E. Müller-Hartmann, Phys. Rev. B **64**, 195114 (2001).
[13] V. Dobrosavljević and G. Kotliar, Phys. Rev. Lett. **78**, 3943 (1997); S. Fujimoto and N. Kawakami, Phys. Rev. B **54**, R11 018 (1996).
[14] H. von Löhnesysen, Philos. Trans. R. Soc. London, Ser. A **356**, 139 (1998).
[15] J. G. Massey and M. Lee, Phys. Rev. Lett. **75**, 4266 (1995).
[16] J. S. Lee, Y. S. Lee, T. W. Noh, S.-J. Oh, J. Yu, S. Nakatsuji, H. Fukazawa, and Y. Maeno, Phys. Rev. Lett. **89**, 257402 (2002).
[17] I. H. Inoue, I. Hase, Y. Aiura, A. Fujimori, Y. Haruyama, T. Maruyama, and Y. Nishihara, Phys. Rev. Lett. **74**, 2539 (1995); H. Makino, I. H. Inoue, M. J. Rozenberg, I. Hase, Y. Aiura, and S. Onari, Phys. Rev. B **58**, 4384 (1998).
[18] D. D. Sarma, A. Chainani, S. R. Krishnakumar, E. Vescovo, C. Carbone, W. Eberhardt, O. Rader, Ch. Jung, Ch. Hellwig, W. Gudat, H. Srikanth, and A. K. Raychaudhuri, Phys. Rev. Lett. **80**, 4004 (1998); A. Chainani, D. D. Sarma, I. Das, and E. V. Sampathkumaran, J. Phys.: Condens. Matter **8**, L631 (1996).
[19] T. Higuchi, T. Tsukamoto, K. Kobayashi, Y. Ishiwata, M. Fujisawa, T. Yokoya, S. Yamaguchi, and S. Shin, Phys. Rev. B **61**, 12 860 (2000); F. M. F. de Groot, J. Faber, J. J. M. Michiels, M. T. Czyżyk, M. Abbate, and J. C. Fuggle, *ibid.* **48**, 2074 (1993).
[20] M. Cardona, Phys. Rev. **140**, A651 (1965).
[21] J. S. Lee, Y. S. Lee, T. W. Noh, K. Char, J. Park, S.-J. Oh, J.-H. Park, C. B. Eom, T. Takeda, and R. Kanno, Phys. Rev. B **64**, 245107 (2001).
[22] J. Okamoto, T. Mizokawa, A. Fujimori, I. Hase, M. Nohara, H. Takagi, Y. Takeda, and M. Takano, Phys. Rev. B **60**, 2281 (1999); P. A. Cox, R. G. Egdell, J. B. Goodenough, A. Hamnett, and C. C. Naish, J. Phys. C **16**, 6221 (1983).
[23] G. Cao, S. McCall, M. Shepard, J. E. Crow, and R. P. Guertin, Phys. Rev. B **56**, 321 (1997).
[24] J. S. Dodge, C. P. Weber, J. Corson, J. Orenstein, Z. Schlesinger,

J. W. Reiner, and M. R. Beasley, Phys. Rev. Lett. **85**, 4932 (2000).

[25] P. Kostic, Y. Okada, N. C. Collins, Z. Schlesinger, J. W. Reiner, L. Klein, A. Kapitulnik, T. H. Geballe, and M. R. Beasley, Phys. Rev. Lett. **81**, 2498 (1998).

[26] M. S. Laad and E. Müller-Hartmann, Phys. Rev. Lett. **87**, 246402 (2001).

[27] L. Capogna, A. P. Mackenzie, R. S. Perry, S. A. Grigera, L. M. Galvin, P. Raychaudhuri, A. J. Schofield, C. S. Alexander, G. Cao, S. R. Julian, and Y. Maeno, Phys. Rev. Lett. **88**, 076602 (2002).

[28] L. Miéville, T. H. Geballe, L. Antognazzab, and K. Char, Appl. Phys. Lett. **70**, 126 (1997).

[29] J. S. Ahn, J. Bak, H. S. Choi, T. W. Noh, J. E. Han, Y. Bang, J. H. Cho, and Q. X. Jia, Phys. Rev. Lett. **82**, 5321 (1999).

[30] K. Hong, S.-H. Kim, Y.-J. Heo, and Y.-U. Kwon, Solid State Commun. **123**, 305 (2002).

[31] H. D. Zhou and J. B. Goodenough, Phys. Rev. B **69**, 245118 (2004).

[32] E. Abrahams, P. W. Anderson, D. C. Licciardello, and T. V. Ramakrishnan, Phys. Rev. Lett. **42**, 673 (1979).

[33] I. Orgzall, B. Lorenz, S. T. Ting, P.-H. Hor, V. Menon, Ch. R. Martin, and H. D. Hochheimer, Phys. Rev. B **54**, 16 654 (1996).

[34] R. M. Hill, Phys. Status Solidi A **34**, 601 (1976); **35**, K29 (1976).

[35] In the VRH formalism of $\rho(T)=\rho_0 \exp[(T_0/T)^{1/(n+1)}]$ the exponent $1/(n+1)$ can be determined by the slope of the $\log[d\log(\rho)/d\log(1/T)]$ vs $\log(T)$ plot (see Refs. 15 and 38). In our fitting processes of Mott VRH and E-S VRH, we made sure that the exponent values should be same with the slopes in those plots. And with additional $1/\sqrt{T}$ and $1/T$ terms (see Refs. 33 and 37), we could get better fitting curves.

[36] A. L. Efros and B. I. Shklovskii, J. Phys. C **8**, L49 (1975).

[37] D.-H. Shin, C. E. Becker, J. J. Harris, J. M. Fernández, N. J. Woods, T. J. Thornton, D. K. Maudek, and J.-C. Portalk, Semicond. Sci. Technol. **14**, 762 (1999); A. Briggs, Y. Guldner, J. P. Vieren, M. Voos, J. P. Hirtz, and M. Razeghi, *ibid.* **27**, 6549 (1983).

[38] J.-J. Kim and H. J. Lee, Phys. Rev. Lett. **70**, 2798 (1993).

[39] K. Pucher, J. Hemberger, F. Mayr, V. Fritsch, A. Loidl, E.-W. Scheidt, S. Klimm, R. Horny, S. Horn, S. G. Ebbinghaus, A. Reller, and R. J. Cava, Phys. Rev. B **65**, 104523 (2002).

[40] D. N. Basov, B. Dabrowski, and T. Timusk, Phys. Rev. Lett. **81**, 2132 (1998).

[41] G. Tzamalis, N. A. Zaidi, C. C. Homes, and A. P. Monkman, Phys. Rev. B **66**, 085202 (2002); Y. Chang, K. Lee, R. Kiebooms, A. Aleshin, and A. J. Heeger, Synth. Met. **105**, 203 (1999); K. Lee, A. J. Heeger, and Y. Cao, Phys. Rev. B **48**, 14 884 (1993).

[42] In this complex system with both disorder and correlation effects, the conductivity maximum energy is not simply determined. Particulary in the small x region, the electron correlation should also involve in this conductivity maximum behavior (see Ref. 12).

[43] R. F. Milligan, T. F. Rosenbaum, R. N. Bhatt, and G. A. Thomas, in *Electron-Electron Interactions in Disordered Systems*, Modern Problems in Condensed Matter Science Vol. 10, edited by A. L. Efros and M. Pollak (North Holland, Amsterdam 1985), pp. 231–286.

[44] T. G. Castner, N. K. Lee, G. S. Cieloszyk, and G. L. Salinger, Phys. Rev. Lett. **34**, 1627 (1975); Y. Imry, Y. Gefen, and D. J. Bergman, Phys. Rev. B **26**, 3436 (1982); C. Y. Chen, N. W. Preyer, P. J. Picone, M. A. Kastner, H. P. Jenssen, D. R. Gabbe, A. Cassanho, and R. J. Birgeneau, Phys. Rev. Lett. **63**, 2307 (1989).

[45] H. S. Choi, J. S. Ahn, J. H. Jung, T. W. Noh, and D. H. Kim, Phys. Rev. B **54**, 4621 (1996); H. J. Lee, J. H. Jung, K. W. Kim, M. W. Kim, T. W. Noh, Y. J. Wang, W. N. Kang, E.-M. Choi, H.-J. Kim, and S.-I. Lee, *ibid.* **65**, 224519 (2002).

[46] K. K. Saha, T. Saha-Dasgupta, A. Mookerjee, S. Saha, and T. P. Sinha, J. Phys.: Condens. Matter **14**, 3849 (2002).

[47] R. Ohara, T. Schimizu, K. Sano, M. Yoshiki, and T. Kawakubo, Jpn. J. Appl. Phys., Part 1 **40**, 1384 (2001); T. Shimizu and T. Kawakubo, Jpn. J. Appl. Phys., Part 2 **40**, L117 (2001).

[48] M. Abbate, J. A. Guevara, S. L. Cuffini, Y. P. Mascarenhas, and E. Morikawa, Eur. Phys. J. B **25**, 203 (2002).

[49] R. F. Bianchi, J. A. G. Carrió, S. L. Cuffini, Y. P. Mascarenhas, and R. M. Faria, Phys. Rev. B **62**, 10 785 (2000).

[50] A. V. Puchkovy, D. N. Basov, and T. Timusk, J. Phys.: Condens. Matter **8**, 10049 (1996).

[51] In a real bialloy system of $A_{1-x}B_x$, random spatial distribution of two-kind atoms could produce additional distribution of ϵ_i around ϵ_A and ϵ_B. This may change the disorder strength Δ from $\Delta_0=\epsilon_A-\epsilon_B$ depending on x.

[52] While the Coulomb interactions are given in a various way under the consideration of the multiplicity effect in the orbitally degenerate Hubbard model, the U value here corresponds to the multiplet-averaged Coulomb interaction.

[53] B. Velický, S. Kirkpatrick, and H. Ehernreich, Phys. Rev. **175**, 747 (1968).

[54] B. J. Yang and J. Yu, (private communication).

[55] P. Soven, Phys. Rev. **156**, 809 (1967); K. I. Wysokiński, Phys. Rev. B **60**, 16 376 (1999); R. Vlaming and D. Vollhardt, *ibid.* **45**, 4637 (1992).

[56] Possible changes in the relative position of each subband are ignored.

[57] J. Kroha, Physica A **167**, 231 (1990).

[58] H. Shima and T. Nakayama, Phys. Rev. B **60**, 14 066 (1999).

[59] J. H. Davies, P. A. Lee, and T. M. Rice, Phys. Rev. B **29**, 4260 (1984).